3rd International Rotating Equipment Conference (IREC)
Pumps, Compressors and Vacuum Technology
Düsseldorf, 14 – 15 September 2016

Design and testing of radial gas bearings with porous media, using fiber-reinforced C/C composites

Sebastian Fleder [1], Björn Gwiasda [1], Martin Appel [1], Prof. Dr.-Ing. Martin Böhle [1], Markus Ortelt [2], Dr.-Ing. Hermann Hald [2]

[1] Technical University Kaiserslautern, Institute of Fluid Mechanics, Gottlieb-Daimler-Strasse, 67663 Kaiserslautern, Germany

[2] German Aerospace Center (DLR), Pfaffenwaldring 38-40, 70569 Stuttgart, Germany

Summary

Journal bearings are used in a large variety of turbomachinery and linear actuators. The bearings can be lubricated using the working fluid or gas. This reduces the maintenance cost and time and the working fluid is not polluted, which reduces the efforts needed in the facility, e.g. oil separator or filter systems. The theory behind radial porous gas bearing design and the function principals are briefly explained. The material properties and special features of the newly developed C/C composite material are explained and the advantages of such a material in comparison to traditional porous gas bearing materials such as copper or other metals are shown. Preliminary investigations are presented to determine the material properties such as the porosity and the resistance coefficients. The test-facility and the results of these investigations is presented and the significance of the results on the bearing design is shown. Substantial advantages of the composite material consist of natural inherent micro-porosity, individually adjustable by the manufacturing process, and accordingly of the capability of an easy lubricant diffusion profile optimisation along the sliding surface, even differing inside the bearing-shell itself. The carbon fiber-reinforcements maintain the dry-running safety of traditional carbon bearings, but supply enhanced resistance to prevent material removal in case of dry run without damaging the runner. A test rig for bearing tests is shown and a variety of tests for the bearings are performed. The tests focus on the maximum load a bearing can carry for different operating parameter such as different rotating speeds, gases, supply pressures or gap sizes. Secondary the influence of the pressure ratio between the supply pressure and the ambient pressure on the load capacity is investigated. In addition to the maximum load, it is examined when turbulent flow occurs in the bearing. The influence of turbulent and laminar flow on the load capacity and the pneumatic stability is pointed out. To improve the data base, the behavior for constant loads and various supply pressures as well as ambient pressures is shown. These investigations allow a target-specific design for low power-loss bearings in different applications, such as turbo-compressors e.g. for heat pumps or chillers and other electric devices like high-speed motors. The gas lubrication allows a much larger rotational speed with low power consumption in comparison to liquid lubricants. Applications with rotational speeds much larger than 10,000, up to 150,000 RPM emerge to be possible. The tests are performed with car-

bondioxide, nitrogen and air, as these are gases usually used in heat-pump, chiller or aerospace applications.

Introduction

Bearings are necessary components in basically all turbomachinery and wherever a relative movement between two components has to be performed within a certain accuracy. When the relative movement between the parts is fast, the use of contact-free support is a good choice.
The bearings presented in this paper are manufactured using a material primarily developed for transpiration cooling for rocket thrust chambers. The advantages of the material are the micro-porosity, which provides a very homogenous fluid film for the support and prevents from hydrodynamic instabilities such as pneumatic hammer.
The theory behind flow through porous media is shortly explained. The manufacturing and some more details about the material is explained. The flow characteristics and resistance parameters for the bearings are determined in an experiment and a validation of laminar and turbulent flow. In additional experiments, some main influences on the bearing load capacity are pointed out. During the research on a feasibility study for the use of porous media, the possibility to optimize the lubrication amount is discovered.

Theoretical overview and background

Overview

Slide bearings are often used for pumps and compressors because of the easy design and the little need of space.
They can be classified into dynamic-acting and static-acting bearings, lubricated with compressible or incompressible fluids. The main difference between dynamic-acting and static-acting is the way the pressure, to carry the existing load, is build up. Dynamic operating slide bearings generate the pressure because of the relative motion between two surfaces. This concept is totally independent from an external pressure supply. Static-acting bearings are fed by an external pressure source. They provide pressure to carry the load even at no speed of the shaft. This is one advantage of static-acting bearings. There will be no wear because of the contact between the rotating shaft and the non-moving bearing surface, like in the case of low speed at starting conditions for dynamic-acting bearings. [POW71]
The direction of the acting force is another category to classify bearings. Bearings to carry load in axial direction are called thrust bearings. Journal bearings can carry load in radial direction. [ROW12]
Static acting journal bearings will be part of the following investigations.
The system which feeds the static acting bearings with fluid is important and has to be designed exactly. [ROW12]
Static acting bearings can mainly be categorized by the underlying feeding system. Groups of feeding systems are single-jet-bearings, multiple-jet-bearings, surface-distributed-micro-jet-bearings and bearings consisting of porous material. With increasing the number of jets distributed over the bearing surface, the load carrying capacity also increases. Surface-distributed-micro-jet-bearings have the best possible load capacity for a given bearing surface compared with the other feeding systems. But they are expensive to produce. [BAR93]
Porous bearings with special treatment of the surface can be designed as bearings with surface-distributed-micro-jet. But these are also expensive to produce. [KOE85]

General theoretical background for porous bearings

Non machined porous material is one big feeding system with a good compromise of manufacturing coast and bearing properties. [BAR93]
To describe the flow through a porous media Darcy [DAR56] defined a well-funded law based on experimental investigations for incompressible fluids. [BAE10]

$$v = -\frac{k_d}{\mu}\left(\frac{\partial p}{\partial x}\right)$$

This equation is only valid for laminar flow conditions within the material.
To consider turbulent flow conditions Forchheimer extend the Darcy equation. [KNE14]

$$\Delta p = -\frac{\mu}{k_d} v - k_f \frac{\rho}{2} v^2$$

To solve the Darcy-Forchheimer equation, for numerical investigation of porous material, the coefficients k_f and k_d, which are material parameters and independent from the working fluid, shown above must be determined.
The required coefficient can be defined with the data from experiments. In case of laminar flow k_f can be neglected.
Experiments although deliver the maximum load capacity for different boundary conditions.
It is important that the available flow conditions are known because only at turbulent flow conditions the Darcy-Forchheimer equation is valid and k_d and k_f can both be determined exactly.
To generate the required flow condition gas bearings will be accomplished for the experiments. Producing turbulent flow is much easier, in the present test setup, for compressible fluids than for incompressible fluids. In case of incompressible fluids, mainly with much larger viscosities and densities than the compressible ones, the coefficients k_d and k_f derived from the tests with compressible fluids can be used. As a result of the higher density and viscosity, the Reynolds number is smaller and therefore the flow inside will be purely laminar. When analyzing the incompressible flow, the Forchheimer coefficient can be neglected, which simplifies the calculation procedure for the bearings.
Porous bearings used in pumps flowed with incompressible fluids will be considered at the numerical investigation of the porous material, as an experimental investigation is impossible due to limitations of the test rig, explained later in chapter “Bearing tests and results”. The numerical investigations use the material coefficients k_d and k_f established for the considered porous media.

Theoretical background for porous gas bearings
To examine the flow condition for compressible flow, the volume flow can be considered through a porous media as a function of $p_s^2 - p_a^2$ or $p_s - p_a$. If the volume flow increases linear over $p_s^2 - p_a^2$ the flow inside the porous media is laminar. A linear increase of the volume flow over $p_s - p_a$ implies a turbulent flow inside the material. [BAR93]
Schmidt [SCH72] shows the context between volume flow and pressure difference by having the density as a function of the pressure include in the Darcy equation for stationary conditions.

$$v = -\frac{k_d}{\mu} grad(P_p)$$

The pressure potential is defined with:

$$X = \int \rho \, dP_p$$

Using the ideal gas equation to define an equation for the density as a function of pressure. Integration of the equation and use of boundary conditions lead to:

$$P_p^2 = P_s^2 - \frac{x_p}{L_p}(P_s^2 - P^2)$$

Differentiate this equation and use $\frac{\partial P_p}{\partial x}$ for the Darcy equation to define an equation for the velocity at the inlet of the porous media

$$v_{in} = \frac{k_d}{\mu} \frac{P_s^2 - P^2}{2 L_p P_s}$$

Considering the turbulent influence

$$\frac{\partial P_p}{\partial x_p} = \underbrace{d_1 v}_{laminar} + \underbrace{d_2 v^2}_{turbulent}$$

A general equation to describe the flow can be deduced with $d_2 = \frac{\rho}{\tau}$ and $d_1 = \frac{k_d}{\mu}$. All constant values are summarized in constant K.

$$\rho v = K_\sigma P_s^{1/\sigma} \left(1 - \frac{1}{\sigma}(\frac{P}{P_s})^2\right)$$

Laminar $\sigma = 1$
Turbulent $\sigma = 2$

Distinguish the laminar and turbulent part lead to the equations in which the linear increase of the flowrate or the velocity as a function of the defined pressure differences can be seen, with $P = P_a$.

Laminar

$$\rho v = K_1(P_s^2 - P_a^2)$$

Turbulent

$$\rho v = K_2 P_s(1 - 1/2(\frac{P_a}{P_s})^2)$$

A detailed derivation is shown in [SCH72].

Figure 1 and Figure 2 show the solution of the laminar and turbulent equation for a constant pressure P_a, a random value for the constant value K and different values for P_s. It can be seen that the flow rate increases linear over $p_s^2 - p_a^2$ for the laminar equation. For the turbulent equation the flow rate increase linear over $p_s - p_a$. This behavior confirms the previously made assumption. The flow conditions within the porous media can be determined safely with this shown effect.

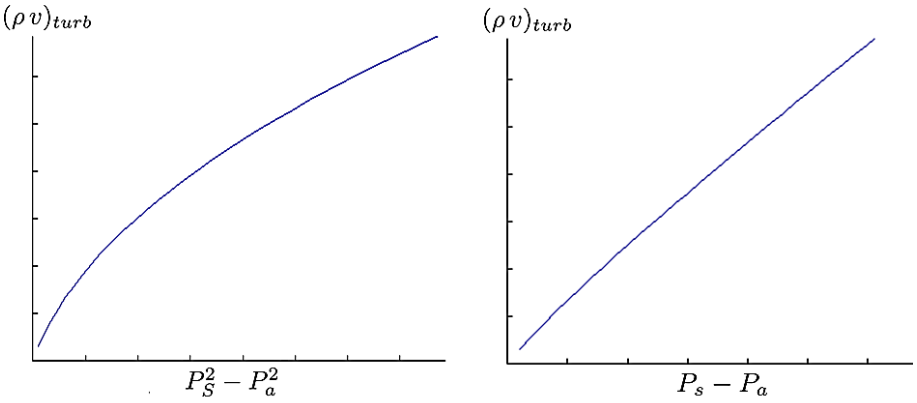

Figure 1 Flowrate - turbulent equation

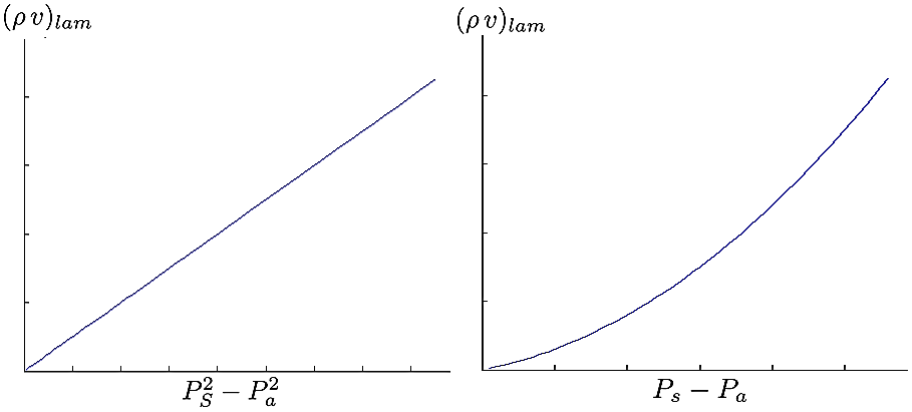

Figure 2 Flowrate - laminar equation

Material Description

The current experience level of transpiration operated CMC structures was achieved by various researches in the field of transpiration cooled ceramic rocket thrust chambers, where porous CMCs were implemented as inner liner material [GRE13], [ORT14], [GRE14], [FRI14], [HAL03]. Depending on the manufacturing process discrete porosities can be created. Referring to optimized hydrogen diffusion due to experience in cryogenic rocket thrust chamber tests porosities in the range from 6 % to 10 % seemed to be the best fit.

Ceramic Matrix Composites (CMC) and structures

For the production of lightweight ceramic structures, the institute of structures and design at DLR Stuttgart works on new materials and processes. The developed components feature high thermal resistance, for this material class high mechanical strength, and low specific weight. Examples include components for stationary and gas turbines, thermal protection systems for spacecraft, high-performance break discs for passenger cars, and aircraft propellers.
The field of research creates new fibre-ceramic material variants and construction methods. Preform techniques such as winding or lamination and autoclave, RTM (Resin Transfer Moulding) and press technology are used to produce fibre-reinforced structures mainly based on carbon, silicon carbide and oxide fibres. The subsequent conversion to ceramics is carried out in special pyrolysis and liquid metal infiltration furnaces.

C/C (carbon fibre reinforced carbon) as an excellent fluid-dynamic reference material for bearing shells

The raw material, a carbon fibre lay-up drenched with a phenolic resin pre-curser is exposed to a high temperature autoclave process. Subsequently the pyrolysis yields a porous pre-form characterized by mass and volume loss and crack creation (***Figure 3***). The final material properties, i.e. fibre matrix bonding, porosity, ductility, strength or pore size, can be influenced varying either, the raw material and the pre-curser or modifying process parameters. C/C represents the material with the currently most scientific experience concerning active transpiration methodology.

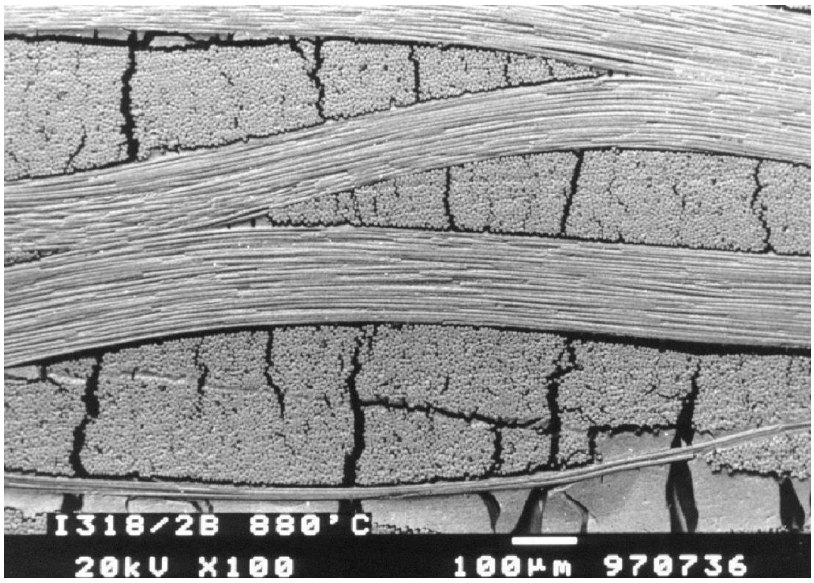

Figure 3: SEM graph of the C/C micro-structure.

C/C seems to be very interesting for transpiration bearing shells because it consists only of carbon fibre and amorphous carbon. Carbon material itself shows good friction behaviour combined with

metallic shafts. The morphology of the transpiration operated CMC materials in general is an important characteristic with regard to homogeneous porosity and permeability.

Part manufacturing

Cylindrical scientific specimens (***Figure 4***) or concrete ring-shaped bearing shells will be extracted from flat raw material plates.The manufacturing of flat plates guaranties high level of reproducible material quality.

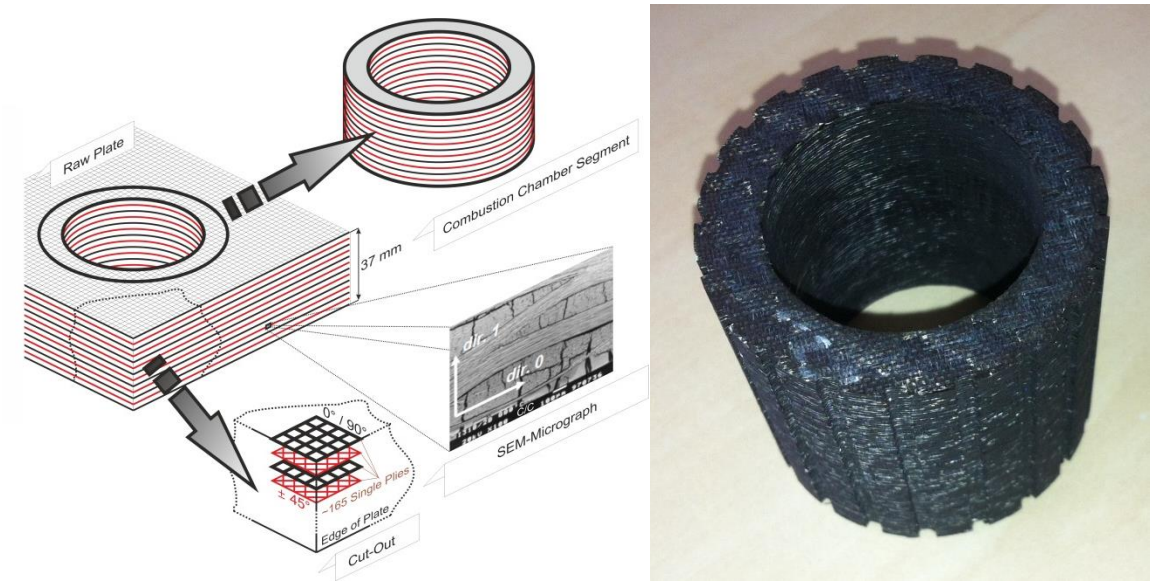

Figure 4: Manufacturing of CMC specimens or ring-shaped bearing shells.

The material orthotropy (***Figure 5***) leads to differences in the diffusion quantity, depending on the fibre lay-up orientation.

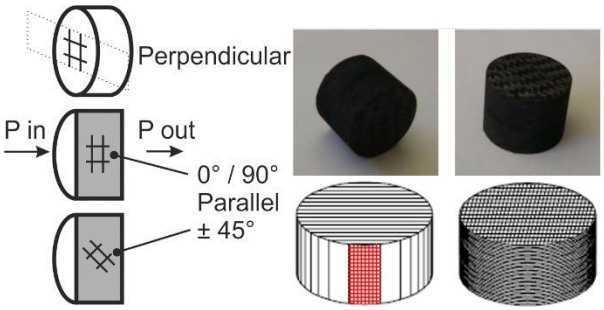

Figure 5: Inherent orthotropic flow directions. Cylindrical specimen size: 30 mm in diameter and height.

Preliminary Investigations and determination of material parameters

At the TU Kaiserslautern a test bench was developed to identify the two parameters k_D and k_F. The probe has a diameter of 10 mm which corresponds to a surface area of 78,54 mm² and is hold in position by a rubber ring. In the lid are several screws to seal the C/C probe from leakages (seen in ***Figure 6***: test bench body).

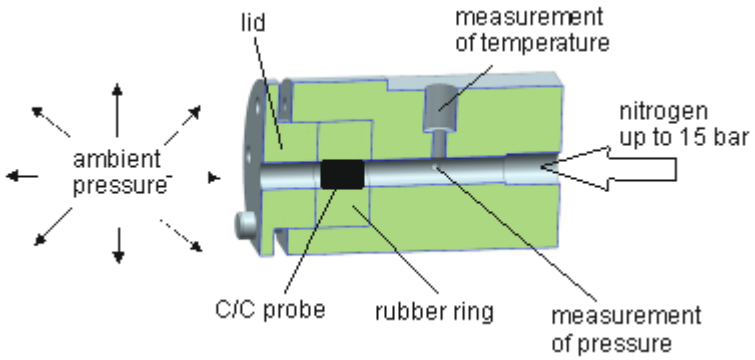

Figure 6: test bench body

The more the screws are tighten the more sealing can be achieved. To make sure that the rubber is not tightened too much an investigation was conducted to make sure the rubber does not leap over the probe inside the channel. This would have an influence on the coefficient, which has to be eliminated.
To recreate the same initial situation a torque wrench was used to tighten all screws with a fixed torque for all other experiments.
Nitrogen is used as working fluid, which is provided by a gas cylinder and can be regulated up to 15 bar towards the Inlet of the test bench. Inside the test bench there are two sensors one for pressure and the other one quantifies the temperature. To control the mass flow rate, a mass flow controller MFC203 from the company Teledyne Hastings is used. The controller has a measurement range from 0 to 50 Normliters per minute. For easier comparison of the results, all data is displayed for g/s instead of normliter per minute.
After the fluid has passed the probe it faces constant ambient pressure. During a measurement process, the mass flow was varied and the pressure and temperature in front of the probe are measured. With the determined parameter pressure and temperature the Darcy-Forchheimer-Equation is calculated and a curve-fitting through all the measured points is performed to identify the parameters k_D and k_F. The formula is shown in the chapter Theoretical Background.
Figure 7 corresponds to the theoretical background in the first chapter and approves the theoretical derivation of the curves. On the left side in ***Figure 7*** at low flow rates and difference pressures the curve starts with a progressive trend and changes to a linear trend. For a precise proof of a turbulent stream inside the probe ***Figure 8*** shows the same trend as introduced in the theoretical background for a turbulent trend.

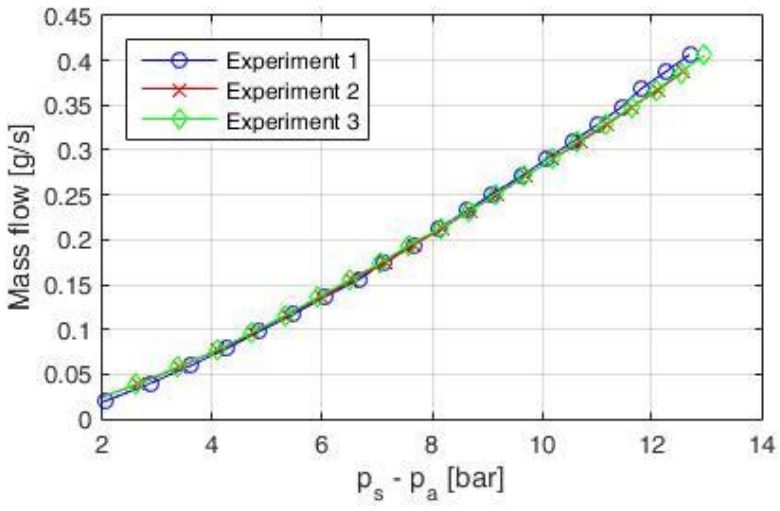

Figure 7: Flow characteristic inside the porous media p_s-p_a

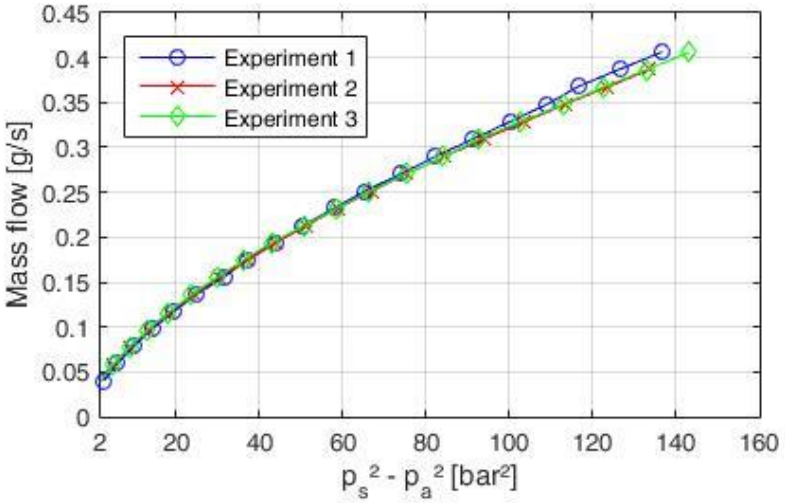

Figure 8: Flow characteristic inside the porous media p_s^2-p_a^2

With this step made, the parameters k_D and k_F are implemented in CFD to perform a numeric investigation. The setup of the simulation, performed using ANSYS CFX 16.1 is summarized in ***Table 1***

Table 1: basic setup CFD Simulation

Attribute	**Physical Value**
Heat transfer	Isothermal
Turbulence model	Shear stress transport (SST)
Time step	Auto timescale
Advection scheme	High resolution
Inlet Condition	Mass flow rate
Outlet Condition	Static pressure

With the results of the mentioned operation steps, a comparison of the consistency of the measured and calculated results with the curve-fitting is possible. The result of the comparison is presented in the figure below.

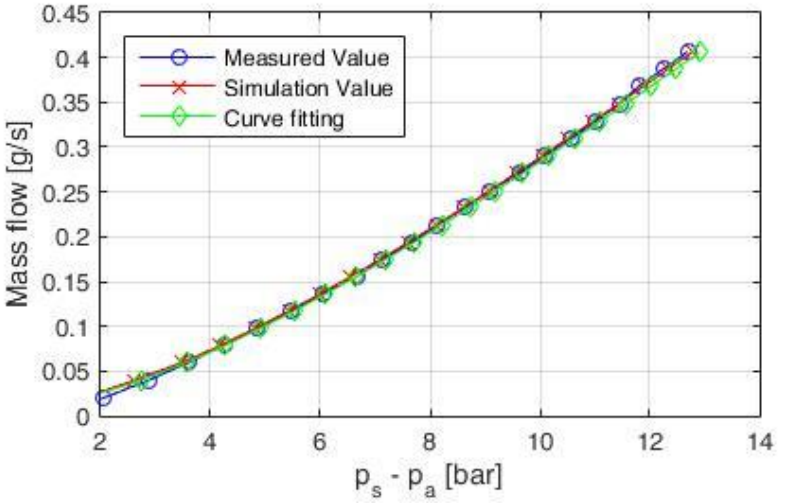

Figure 9: Comparison experiment and CFD

With such a conformance the next step is to predict the pressure drop for a real bearing geometry. ***Figure 10*** shows a picture of the slide bearing geometry.

Figure 10: slide bearing on shaft

The probe for both, the bearing and the test cylinder, is made of the exact same material as the slide bearing in ***Figure 10***. ***Figure 11*** shows the pressure drop inside a real bearing geometry.

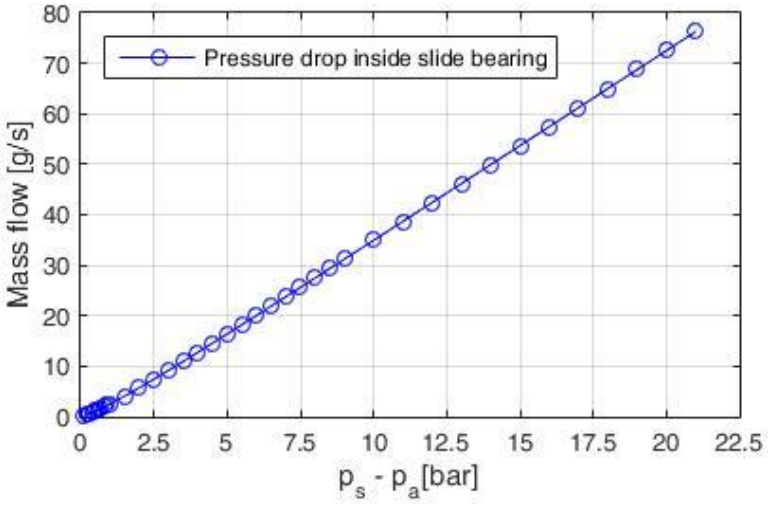

Figure 11: pressure drop inside real geometry

This result can be used to predict and optimize the fluid consumption in the bearing tests.

Bearing Tests and Results

Test Rig

The test rig contains of a DC Motor with a device to measure the current to determine the driving-power of the device. The motor is connected to the test rig with a clutch at Position 3. The shaft inside the test rig is divided in two parts to allow an assembly of the rotor-bearing combination. Each part of the shaft is supported by two roller bearings (4 and 5) to provide sufficient stiffness of the entire assembly. The bearing itself is mounted in a pressure chamber with two hydraulic fittings to connect different tubes for the supply of lubricant. The lubricant flows from the fitting inside an annular space. From there, the lubricant flows inside the channels ion the outer surface of the bearing. The lubricant flows through the bearing and enters the gap between shaft and bearing and leaves the pressure chamber in axial direction through the gap between shaft and bearing. The pressure chamber is connected to a load cell to measure the force applied to the bearing. The force is applied using a hydraulic cylinder (1), operating with pressurized air. The direction of the force and the amount can be set with different valves and a pressure controller and is measured with a load cell (2). The maximum possible force is about 1200N.
The test rig is depicted in ***Figure 12***, a flow scheme inside the bearing casing is depicted in *Figure 13*.

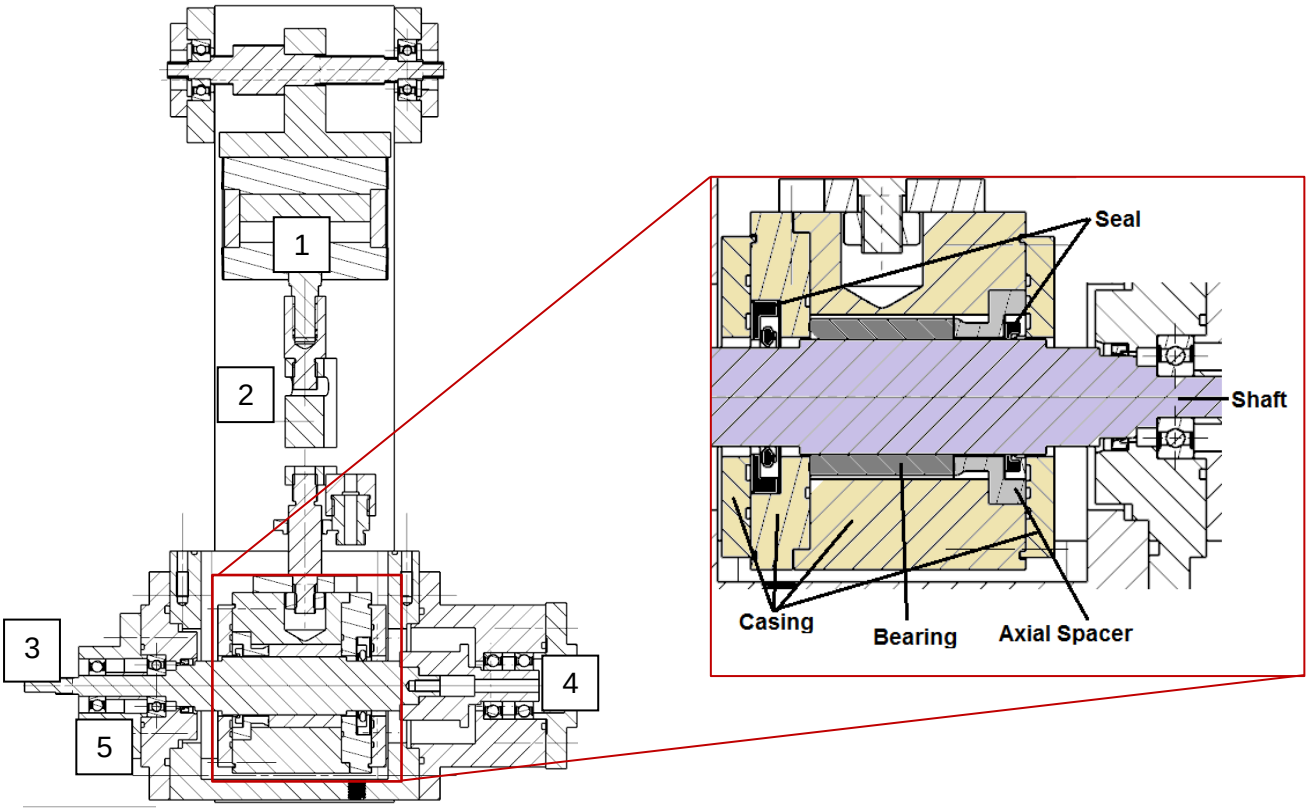

Figure 12: Test Rig

The gas is provided through the inlet port and enters a plenum inside the pressure chamber. Small grooves on the outside of the bearing guide the gas to pressurize the entire outer area of the bearing. The gas is transported through the porous bearing and enters the gap between the shaft and the bearing. The gas flows to the axial outlets at the front and back side of the pressure chamber. To operate the system with variable outlet pressures, it is possible to assemble two rotary seals on the front and back side to guide the gas to the outlet port. For all experiments in this manuscript, the outlet port has been closed and the seals are removed. It is planned to change the outlet pressure to analyze the dynamic bearing behavior and the dynamic stability with changing ambient pressures.

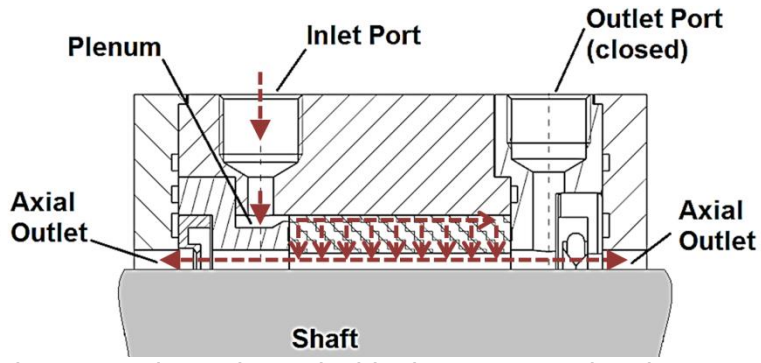

Figure 13: Flow scheme inside the pressure chamber

The motor current is measured with a current-voltage converter. The pressure of the lubricant is measured with a pressure transducer inside a flow box, as well as the temperature, using a PT100 probe. A continuous-flow heater maintains a steady state temperature of 15°C, to prevent the tubes and valves from icing and allow an easier comparison between the measurements.

Measurement

As mentioned before, all tests are performed with gas as working fluid, as the limitations of the pressure piping to lubricate the bearing does not allow lubrication with fluids. For the same flow velocity in the bearing, a liquid incompressible fluid requires higher differential pressures than gases. To reduce the cost and size of the piping, only gases are used, but the results can also be applied for liquid incompressible flow.
For each measurement, the desired rotational speed and the desired feeding pressure of the lubricant is set to a stationary value. The force is applied and rises slowly during the measurement. Each second, ten values for each sensor are recorded and the arithmetic average is calculated. With increasing load, the required driving power rises, until the bearing is running in a stick-slip and later in a dry friction. In this dry friction, the clutch is no longer able to handle the occurring friction and disconnects the motor from the shaft. When analyzing the characteristics of the force-driwing power curve, the dry run point can be determined and therefore the maximum possible load for the bearing can be found.

Results

The power loss characteristics for the same medium and different rotational speeds is depicted in ***Figure 14***.

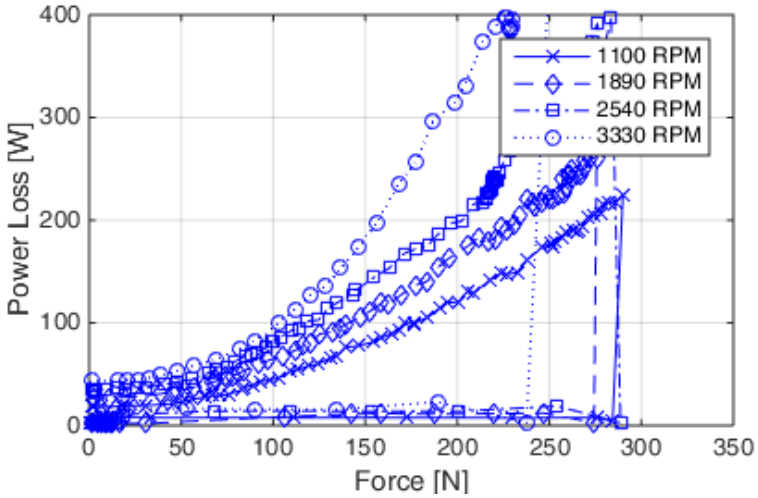

Figure 14: Influence of rotational speed on bearing characteristics

With rising load, the driving power rises as well. Higher rotational speeds need higher driving power. When observing the dimensionless driving power, calculated with

$$P_{Dimensionless} = P_{local} / P_{global\ minimum}$$

$P_{global\ minimum}$ is the global minimum of required driving power, which is located at zero load.
Figure 15 shows the dimensionless driving power as function of the load for the same configuration. The curves are perfectly aligned with each other, resulting in the conclusion that no influence of rotational speed is present. The static effect of the bearing is much larger than the dynamic effect.

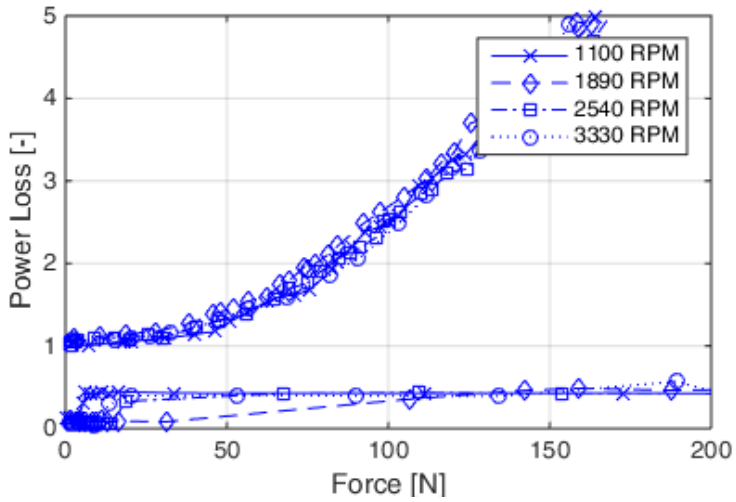

Figure 15: bearing loss characteristics in scope

The influence of feeding pressure is analyzed based on the previous results that the rotational speed has no significant influence. A rotational speed of 1100RPM is chosen for the following measurements. The feeding pressure is set to different values, ranging from pressure ratios of 2 up to 15, described in table 2.

Name	Pressure ratio
Low pressure	2.5
Medium pressure	5
High pressure	7.5
Extreme pressure	15

Table 2: Feeding Pressure ratios

Figure 16 shows the dimensionless power loss as function of the load for the four different feeding pressures.

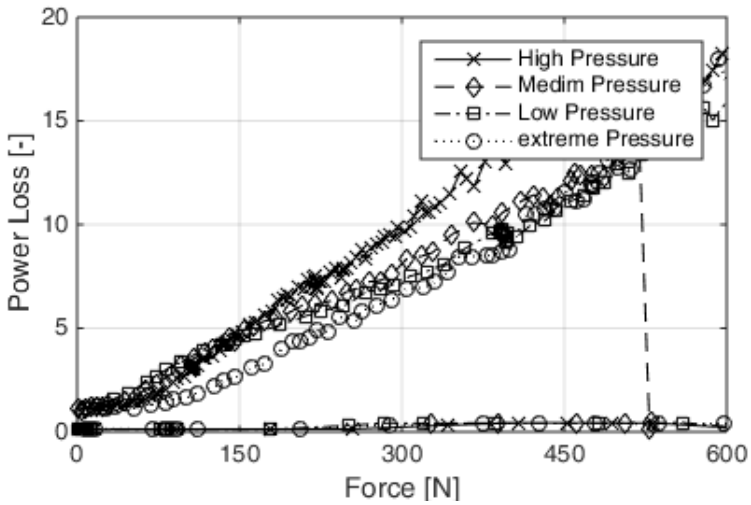

Figure 16: bearing characteristics for different feeding pressures

With rising load, all curves are located close to each other. Only at low loads a significant difference can be seen. Ata certain point, the lines converge to the same slope and the differences become smaller. This point is identified as the point of dry run and therefore the point of maximum possible load. This point also marks a turning point in the slope of the curve (***Figure 17***).

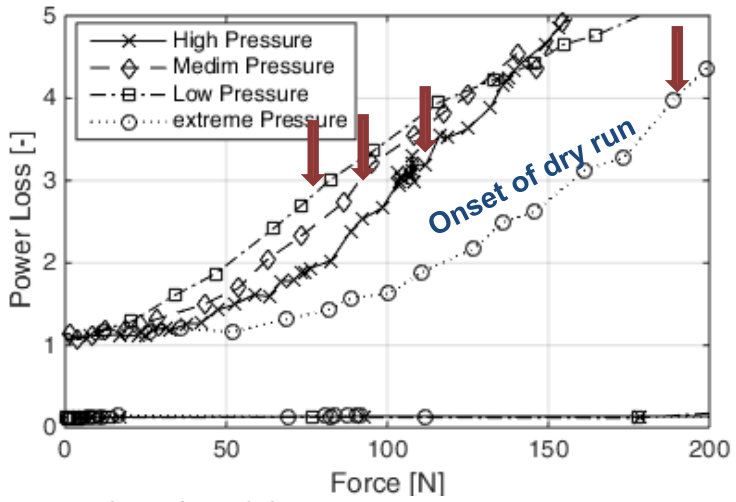

Figure 17: detection of dry run

The influence of different lubricants is analyzed with carbon dioxide, nitrogen and pressurized air. ***Figure 18*** shows the load for different feeding pressures for air, ***Figure 19*** for nitrogen. In comparison to carbon dioxide, the maximum force for the bearing is smaller (***Figure 20***).

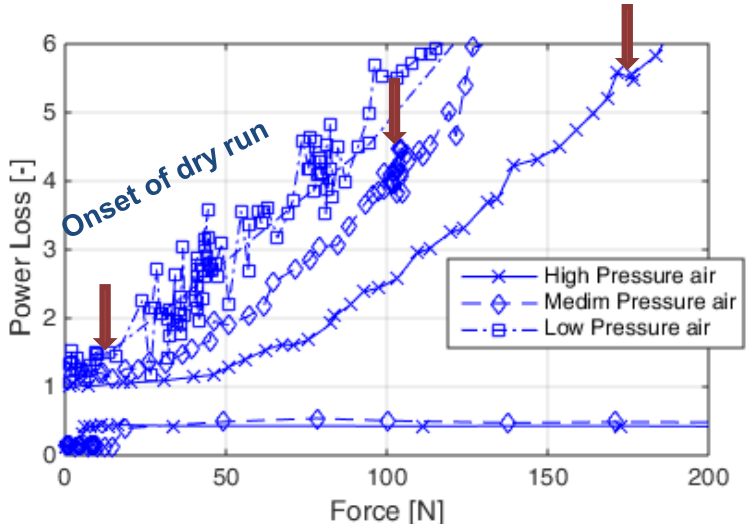

Figure 18: detection of dry run for air

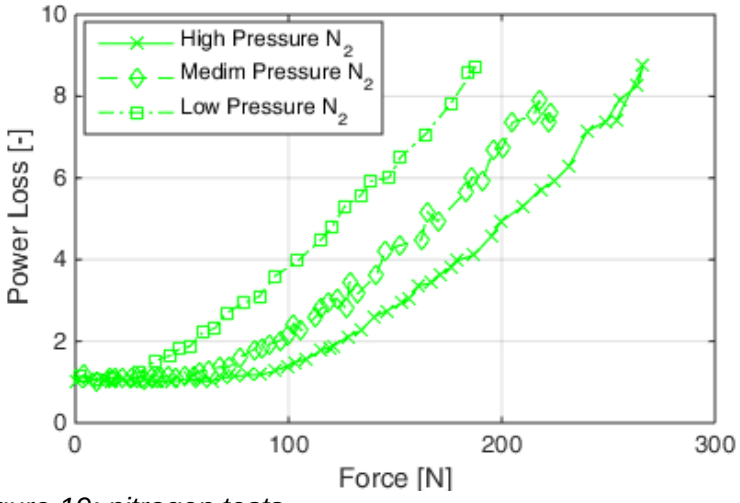

Figure 19: nitrogen tests

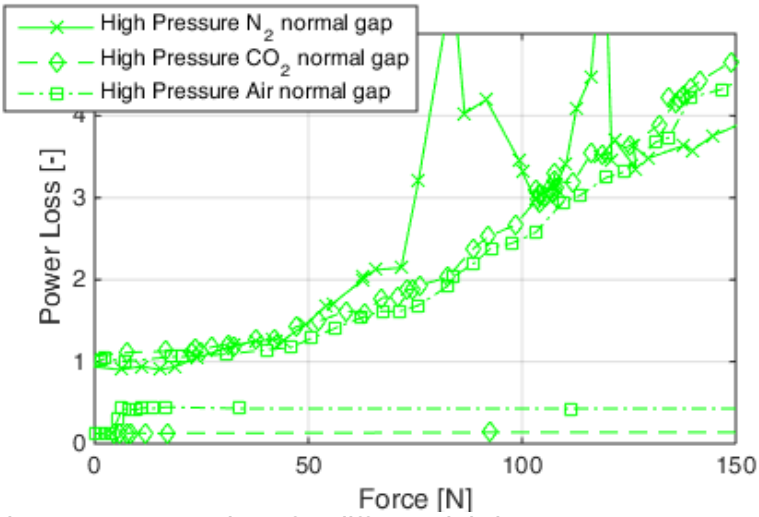

Figure 20: comparison for different lubricants

The effect of gap size is analyzed with the reference gap of 0.1mm compared to the small gap of 0.02mm, which corresponds to a gap-size-ratio of 5. With the small gap, already small forces of under 50N result in material contact and dry run, observable by the rapid increase of driving power and a non-continous slope of the curve (***Figure 21***).

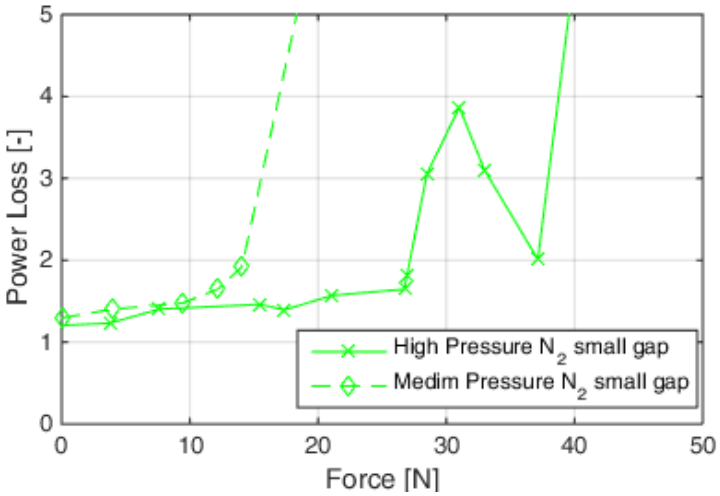

Figure 21: bearing characteristics for small gap size

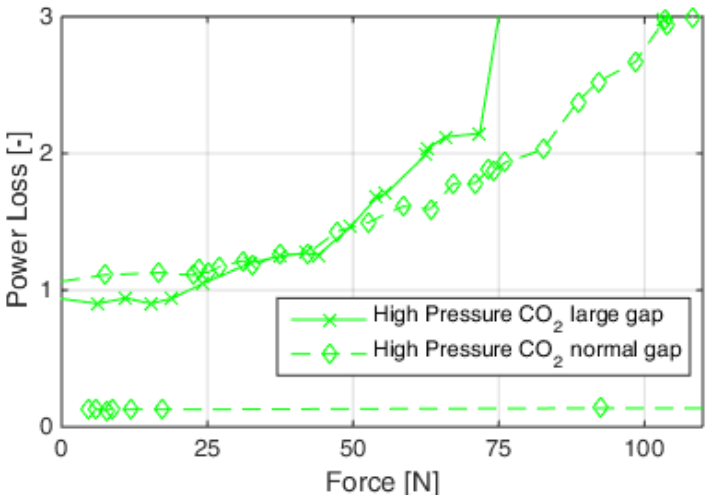

Figure 22: bearing characteristics for large gap size

The results serve to perform a loss reduction analysis for given applications. For a given load and rotational speed, a maximum of feeding pressure should be applied, regardless of the medium. With higher feeding pressure, the losses in the bearing reduce. At the example of the reference clearance with 1100 RPM and a load of 75N, the losses increase about 20% compared to the losses at zero load for a supply pressure ratio of 15. Reducing the ratio to 7.5 results in a power loss rise of factor 1.8 in comparison to the reference at zero load. A further decrease to pressure ratios of 5 or 2.5 result in more than the double power losses, respective a power loss ratio of 2.2 and 2.4.
Never the less, the lubricant consumption needs to be taken into account. Rising feeding pressure ratios lead to higher lubricant mass flows, as predicted in the chapter “Preliminary Investigations and determination of material parameters”. For applications with low specific speed or other restrictions concerning an extremely low flow rate, as well as applications where a high pressure ratio could complicate the assembly, other parts of the product or where safety regulations are very strict, it could be suitable to reduce the feeding pressure to lower values.

Problems during the measurements

Unfortunately, the shaft was damaged during the tests with low clearance, unable to be repaired without destroying the fitting between bearing and shaft, see ***Figure 23***. This results in a lack of high-speed tests and tests with other mediums such as fluids or other gases.

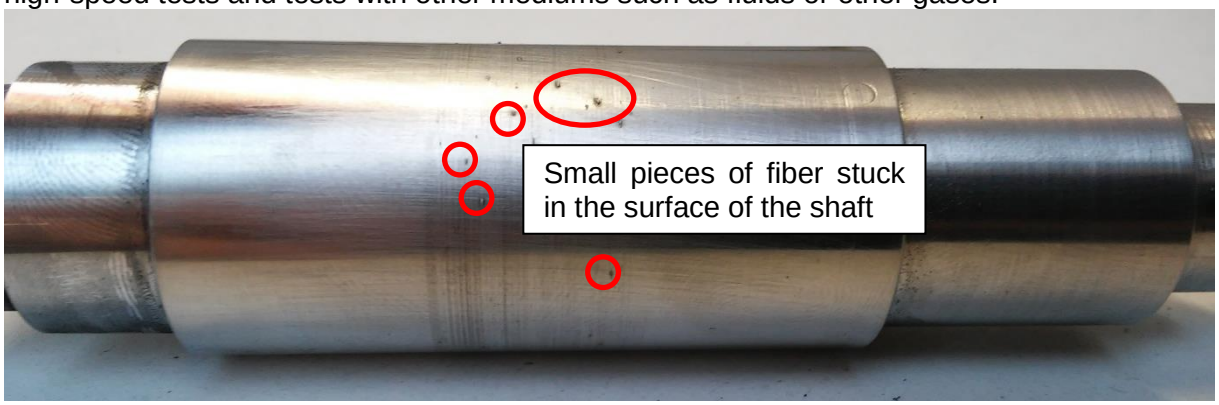

Figure 23: damaged shaft after dry run

Conclusion

The porous bearings seem to be a good solution for applications, where low friction and high speed requirements come together. A higher feeding pressure boosts the performance of the bearing and reduces the losses at stationary operation.
The gap sizes should not be chosen too small, as material contact occurs directly after applying a load. A medium gap size of 0.1mm shows a better performance than a narrow clearance or a too large gap. The bearings can handle both, gas and liquid, to maintain the lubrication.
The manufacturing process of the bearings is highly variable concerning the porosity and other material parameters. A bearing with variable porosity and resistance coefficient is possible and could be applied as a combined axial and radial bearing for some applications. When lower radial loads are present, the feeding channels of the bearing can be faded out to reduce the lubricant massflow over the bearing.

With the successful work on the investigation of the parameter kd and kf a transfer to a numerical investigation was conducted. With the help of numerical calculations new bearing designs can be studied in advance to extensive experimental investigations on a test rig.

It was shown that Porous media bearings with C/C composite material are possible. Further investigations should show if the application of classic design regulations for this material type is valid and determine the limitations concerning stability and lifetime. Additionally, the test rig will be improved to allow measurements with incompressilbe fluids, such as water or different oils to allow

usage in applications such as water supply pumps, hydrocarbon industry or automotive applications such as turbochargers, cooling pumps or fuel pumps.

Figure 24 shows the SEM graph of another important CMC candidate, so-called C/SiCN, which is an alternative material for these kind of application.

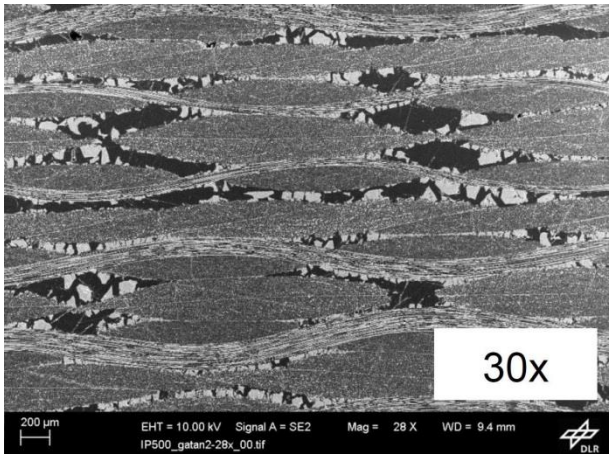

Figure 24: SEM graph of typical DLR's C/SiCN material, showing homogeneous pore distribution and SiCN fractures inside the pores

This material consists of a second matrix fracture represented by small particles of silicon carbide SiC – a real ceramic material fracture, showing high amorphous brittleness. These SiC particles give the material more strength and abrasion robustness, and in form of small particles the brittleness does not affect the overall structural ductility. So C/SiCN was chosen for the transpiration bearing technology as a relevant candidate too, because it shows enough softness against surface contact without brittleness effects.

Acknowledgements
We acknowledge the cooperation with German Aerospace Center, which provided the material and developed the original idea of the application as bearing.
The simulations were executed on the high performance cluster "Elwetritsch" at the TU Kaiserslautern which is part of the "Alliance of High Performance Computing Rheinland-Pfalz" (AHRP). We kindly acknowledge the support.

Literature

[POW71] Powell J. W. : Design of aerostatic bearings. The machinery publishing co. ltd (1971)
[ROW12] Rowe B. W. : Hydrostatic, aerostatic and hybrid bearing design. Elsevier (2012)
[BAR93] Bartz W. J. : Luftlagerung. Expert Verlag (1993)
[KOE85] Koehler H. : Druckgespeiste Gaslager mit flächig verteilten Mikrodüsen. TU München, Diss. (1985)
[DAR56] Darcy H. : Les fontaines publiques de la village de Dijon. Viktor Dalmont (1856)
[BAE10] Baehr H. D. & Stephan K. : Wärme und Stoffübertragung. Springer (2010)
[BAR93] Bartz W. J. : Luftlagerung. Expert Verlag (1993)
[SCH72] Schmidt J. : Berechnung und Untersuchung aerostatischer Radiallager aus porösen Werkstoff. Karlsruhe, Diss (1972)
[KNE14] Kneer A. :Numerische Untersuchung des Wärmeübertragungsverhaltens in unterschiedlichen porösen Medien. Karlsruhe, Diss (2014)
[GRE13] D. Greuel; 2013. Untersuchungen zum Impuls- und Stofftransport in effusiv gekühlten faserkeramischen Raketenbrennkammerwänden. *Dissertation, RWTH Aachen, Germany.*
[ORT14] M. Ortelt, H. Hald, I. Mueller; 2014. Status and future perspectives of the CMC rocket thrust chamber development at DLR. *65th International Astronautical Congress, Toronto, Canada.*

[GRE14] D. Greuel, A. Herbertz, O.J. Haidn, M. Ortelt, H. Hald; 2004. Transpiration cooling applied to C/FC liners of cryogenic liquid rocket emgines. *40th AIAA/ASME/SAE/ASEE/ Joint Propulsion Conference and Exhibit, 11 – 14 July, Fort Lauderdale, Florida.*
[FRI14] D. Fricke, 2014. Vergleichende numerische und experimentelle Untersuchung poroeser durch-stroemter Medien. *Diplomarbeit, DLR IB 435-2014/29. DLR Institute of Structures and Design, Stuttgart, Germany.*
[HAL03] H. Hald, M. Ortelt, I. Fischer, D. Greuel; 2003. CMC Rocket Combustion Chamber with Effusion Cooling. *54th International Astronautical Congress, Bremen, Germany.*

Your contact person:

Thomas Roggel, VDMA Verlag
Phone: +49 69 66 03-1412
Telefax: +49 69 66 03-2412
E-Mail: Thomas.Roggel@vdma.org